

MALDI-MSI and label-free LC-ESI-MS/MS shotgun proteomics to investigate protein induction in a murine fibrosarcoma model following treatment with a vascular disrupting agent

COLE, Laura <<http://orcid.org/0000-0002-2538-6291>>, BLUFF, Joanne E., CAROLAN, Vikki <<http://orcid.org/0000-0001-7384-4018>>, PALEY, Martyn N., TOZER, Gillian M. and CLENCH, Malcolm <<http://orcid.org/0000-0002-0798-831X>>

Available from Sheffield Hallam University Research Archive (SHURA) at:

<http://shura.shu.ac.uk/8227/>

This document is the author deposited version. You are advised to consult the publisher's version if you wish to cite from it.

Published version

COLE, Laura, BLUFF, Joanne E., CAROLAN, Vikki, PALEY, Martyn N., TOZER, Gillian M. and CLENCH, Malcolm (2014). MALDI-MSI and label-free LC-ESI-MS/MS shotgun proteomics to investigate protein induction in a murine fibrosarcoma model following treatment with a vascular disrupting agent. *Proteomics*, 14 (7-8), 890-903.

Copyright and re-use policy

See <http://shura.shu.ac.uk/information.html>



MALDI-MSI and Label Free LC-ESI-MS/MS Shotgun Proteomics to Investigate Protein Induction in a Murine Fibrosarcoma Model following Treatment with a Vascular Disrupting Agent

Journal:	<i>PROTEOMICS</i>
Manuscript ID:	pmic.201300429.R1
Wiley - Manuscript type:	Research Article
Date Submitted by the Author:	n/a
Complete List of Authors:	Cole, Laura; Sheffield Hallam University, Biomedical Research Centre Bluff, Joanne; University of Sheffield, Department of Oncology Carolan, Vikki; Sheffield Hallam University, Biomedical Research Centre Tozer, Gillian; University of Sheffield, Department of Oncology Paley, Martyn; University of Sheffield, Department of Cardiovascular Science Clench, Malcolm; Sheffield Hallam University, Biomedical Research Centre ;
Keywords (free text entry):	vascular disrupting agents, Plectin, CA4P, HSP90, stree induced molecular chaperones

SCHOLARONE™
Manuscripts

1
2
3
4
5
6
7
8
9
10
11
12
13
14
15
16
17
18
19
20
21
22
23
24
25
26
27
28
29
30
31
32
33
34
35
36
37
38
39
40
41
42
43
44
45
46
47
48
49
50
51
52
53
54
55
56
57
58
59
60

1 **MALDI-MSI and Label free LC-ESI-MS/MS Shotgun Proteomics to Investigate Protein Induction in a**
2 **Murine Fibrosarcoma Model following Treatment with a Vascular Disrupting Agent.**

3 ¹Laura M Cole, ²Joanne E Bluff, ¹Vikki A Carolan, ³Martyn N Paley, ²Gillian M Tozer, ¹Malcolm R
4 Clench

5 ¹Biomedical Research Centre. Sheffield Hallam University, Sheffield, S1 1WB.

6 ²Tumour Microcirculation Group, CR-UK/YCR Sheffield Cancer Research Centre, Department of
7 Oncology, University of Sheffield, Sheffield S10 2RX.

8 ³ Department of Cardiovascular Science, University of Sheffield, Sheffield, S10 2JF.

9 **Running Title:** Tumour protein Induction after VDA treatment.

10 **Keywords:** MALDI-MSI, LC-ESI-MS/MS, Plectin, HSP-90, vascular disrupting agents, CA4P, bio-
11 markers, stress induced molecular chaperones

12 **Abbreviations:**

13 ESI-LC-MS/MS: electrospray ionisation-liquid chromatography-tandem mass spectrometry

14 HSP: heat shock protein

15 IHC: immunohistochemistry

16 IMS: ion mobility separation

17 MALDI-IMS-MS: matrix assisted laser desorption ionisation-ion mobility separation-mass
18 spectrometry

19 PMF: peptide mass fingerprint

20 VEGF: vascular endothelial growth factor

21 MudPIT: multidimensional protein identification technology

22

Abstract:

Tumour vasculature is notoriously sinusoidal and leaky, and is hence susceptible to vascular disruption. Microtubule destabilising drugs such as the combretastatins form the largest group of tumour vascular disrupting agents (VDAs) and cause selective shutdown of tumour blood flow within minutes to hours, leading to secondary tumour cell death. Targeting the tumour vasculature is a proven anticancer strategy but early treatment response bio-markers are required for personalising treatment planning.

Protein induction following treatment with combretastatin A4-phosphate (CA4P) was examined in a mouse fibrosarcoma model (fs 188), where tumour cells express only the matrix-bound isoform of vascular endothelial growth factor A (VEGF188). These tumours are relatively resistant to vascular disruption by CA4P and hence a study of protein induction following treatment could yield insights into resistance mechanisms.

The distribution of a number of proteins induced following treatment were visualised by MALDI-MSI. Responses identified were validated by LC-ESI-MS/MS and immunohistochemical (IHC) staining. Significant changes in proteins connected with necrosis, cell structure, cell survival and stress-induced molecular chaperones were identified. Protein-protein interactions were identified using STRING 9.0 proteomic network software. These relationship pathways provided an insight into the activity of the active tumour milieu and a means of linking the identified proteins to their functional partners.

1
2
3
4
5
6
7
8
9
10
11
12
13
14
15
16
17
18
19
20
21
22
23
24
25
26
27
28
29
30
31
32
33
34
35
36
37
38
39
40
41
42
43
44
45
46
47
48
49
50
51
52
53
54
55
56
57
58
59
60

44 **Introduction:**

45 The identification of proteins that provide links to drug mechanisms and relate to
46 sensitivity/resistance is essential for the progression of anti-cancer therapeutics. Early predictive bio-
47 markers for assessing efficacy of drug treatments are required for personalising cancer treatments.
48 The identification of proteins induced after administration of an anti-cancer drug would provide
49 valuable insights into drug treatment response mechanisms. Treatment response is clearly complex
50 and multifactorial but increased knowledge in this area could provide strategies for future
51 combination therapies. A protein induction time course has been studied in a CA4P-treated mouse
52 fibrosarcoma model. It is known that, shortly after administration of CA4P, major shutdown of the
53 tumour vascular network occurs, leading to disruption of the 3D capillary architectural integrity [1].
54 The aim of the proteomic study of regional tumour variations reported here was to advance
55 understanding of tumour progression following treatment with CA4P, as a leading example of a VDA.
56 We chose to use mouse fibrosarcomas that express only the matrix-bound isoform of VEGF (fs188),
57 as these tumours are relatively resistant to CA4P, compared to their counterpart tumours that
58 express the more soluble VEGF isoforms (VEGF120 and 164) [1]. Previously, we observed that
59 proteomic studies of fs120 tumours (expressing only the soluble isoform of VEGF, VEGF120) were
60 compromised by excessive masking of protein induction by very high haemoglobin levels, caused by
61 extensive haemorrhage of the CA4P-sensitive blood vessels [2].
62 Matrix assisted laser desorption ionisation-mass spectrometry imaging (MALDI-MSI) is a unique
63 technique that allows visualisation of the spatial distribution of a particular species, within a
64 biological tissue sample. Multiple single mass spectra can be combined together to generate
65 molecular maps of an ion of interest. MALDI-MSI has been frequently utilised for the direct protein
66 profiling of tumour tissue samples, including tumour margin analysis [3-7]. A commonly used
67 approach to study proteins of high relative molecular mass is the use of “*on-tissue*” tryptic digestion.
68 This is a ‘bottom up’ proteomics approach, which enables the identification of proteins via the

69 resulting tryptic peptides. This method is performed directly on cryo-sectioned tissue samples with
70 the employment of MALDI-MSI. The Images generated reveal the positioning of peptides within the
71 tryptically digested tumour sections [8, 5, 9].

72

73 Here we report the use of LC-ESI-/MS/MS label free quantification of proteins, in conjunction with
74 MALDI-MSI, to study the pharmacodynamic response of mouse fibrosarcomas to the VDA, CA4P. The
75 methodology employed tissue homogenisation, protein extraction, reduction, alkylation and
76 enzymatic digestion of proteins prior to data-dependent LC/MS/MS analysis. The proteomic
77 responses from fs188 tumours (saline-treated controls and tumours 0.5h, 6h, 24h and 72h post-
78 CA4P treatment) were used for LC-ESI-MS/MS and MALDI-MSI analysis, in order to create a time
79 course of data, incorporating the vascular shut-down and tumour recovery phases post-drug
80 administration.

81

82 **Materials and Methods**

83 **Chemicals and Materials**

84 α -Cyano-4-hydroxycinnamic acid (CHCA), aniline (ANI), ethanol (EtOH), chloroform (CHCl_3),
85 acetonitrile (ACN), octyl- α /b-glucoside (OcGlc), tri-fluoroacetic acid (TFA), ammonium bicarbonate,
86 haematoxylin, eosin, xylene and DPX mountant were from Sigma–Aldrich (Dorset, UK). Modified
87 sequence grade trypsin (20 μg lyophilised) was obtained from Promega (Southampton, UK).

88

89 **Tissue samples**

90 All animal procedures were carried out in accordance with the United Kingdom Animals (Scientific
91 Procedure) Act 1986, with local ethics committee approval and following published guidelines for
92 the use of animals in cancer research (Workman *et al.*, 2010). Mice were injected sub-cutaneously in

1
2
393 the rear dorsum with a 50 µl tumour cell suspension containing 1 x 10⁶ fs188 tumour cells in serum-
4
594 free medium. These fibrosarcoma (fs) cells are engineered to express only the VEGF188 isoform of
6
795 vascular endothelial growth factor A (VEGF) [1]. Tumours were allowed to grow to approximately
8
996 500 mm³, before CA4P treatment (a 50 µl single dose of 100 mg/kg i.p in saline). Mice were
10
1197 sacrificed and tumours excised at various times after treatment before being snap frozen in liquid
12
1398 nitrogen-cooled isopentane and stored at -80°C for later processing.
14
15
16
17

18
19
20100 Experimental groups for Principle Component Analysis (PCA) and Partial Least Squares Discriminant
21
22101 Analysis (PLSDA) Controls (saline i.p), n = 4, CA4P (0.5 h after treatment), n = 5, CA4P (6 h after
23
24102 treatment), n = 5, CA4P (24 h after treatment), n = 5, CA4P (72 h after treatment) n = 4,.
25
26
27103
28
29

30104 **Tissue preparation**

31
32105 10 µm-thick frozen tissue sections were cut, using a Leica CM3050 cryostat (Leica Microsystems,
33
34106 Milton Keynes, UK). The sections were then freeze-thaw mounted on poly-L-lysine glass slides.
35
36107 Mounted slides were either used immediately or stored in an airtight tube at -80 °C for subsequent
37
38108 use.
39
40

41109 ***In situ* tissue digestion and trypsin deposition**

42
43110 The tissue samples were washed initially with 70% and then 90% ethanol for 1 min then left to dry.
44
45111 Subsequently, slides were immersed in chloroform for 10 s. Prior to matrix application, *in situ* tissue
46
47112 digestion was performed with trypsin solution prepared (from lyophilised trypsin), at 20 µg/ml, by
48
49113 addition of 50 mM ammonium bicarbonate (NH₄HCO₃) pH 8, containing 0.5%octyl-a/b-glucoside
50
51
52114 (OcGlc).
53
54
55
56
57
58
59
60

1
2
3 115 The “Suncollect” (SunChrom, Friedrichsdorf, Germany) automatic pneumatic sprayer was used to
4
5 116 spray trypsin in a series of layers. The sections for MALDI-MS and MALDI-MSI were incubated in a
6
7 117 humidity chamber containing H₂O 50%: methanol 50% overnight at 37°C and 5% CO₂.
8
9
10
11 118

12 13 119 **Methods and instrumentation**

14
15 120 The matrix, α -cyano-4-hydroxycinnamic acid (CHCA) and aniline in acetonitrile:water:TFA (1:1:0.1 by
16
17 121 volume), was applied using the Suncollect (at 5 mg/ml) in a series of 5 layers. For trypsin and CHCA,
18
19 122 each layer was sprayed at 3 μ l/min.. Identical coordinate settings to those used for trypsin deposition
20
21 123 were employed, to ensure sample uniformity. Equimolar amounts of aniline were added to the CHCA
22
23 124 solution, i.e. 1 ml of 5 mg/ml CHCA solution contained 2.4 μ l of aniline.
24
25
26

27 125 MALDI- IMS/MS, MALDI- IMS/MSI and MALDI- IMS-MS/MS were performed using a HDMS SYNAPT™
28
29 126 G2 system (Waters Corporation, Manchester, UK) and Driftscope 2.1 software (Waters Corporation,
30
31 127 UK). In order to achieve good quality MS/MS spectra, they were acquired manually moving the laser
32
33 128 position and adjusting the collision energy to achieve good signal to noise for product ions across the
34
35 129 full m/z range of the spectrum. Collision energies were adjusted from 70 to 100 eV during
36
37 130 acquisition and acquisition times were generally of the order of 5–10 s per spectrum. MS/MS spectra
38
39 131 were uploaded to perform a Mascot (Matrix Science, London, UK) search, which used the UniProt
40
41 132 database in order to generate a sequence match. Image acquisition was performed using raster
42
43 133 imaging mode at 30-100 μ m spatial resolution, Biomap 3.7.5.5 software (<http://www.maldi->
44
45 134 [msi.org/](http://www.maldi-msi.org/)) was used for image generation. To enable simple visual comparison between images all
46
47 135 data were normalised to m/z 877/ m/z 1066 (peaks arising from the α CHCA matrix).
48
49
50

51
52 136 LC-ESI-MS/MS analyses were performed with a Bruker nanoESI source fitted with a steel needle
53
54 137 using Ion spray voltage of 1500V. MS/MS was acquired using the following AutoMSMS settings: MS:
55
56 138 0.5 s (acquisition of survey spectrum), MS/MS (CID with N₂ as collision gas): ion acquisition range:
57
58
59
60

1
2
3
4
5
6
7
8
9
10
11
12
13
14
15
16
17
18
19
20
21
22
23
24
25
26
27
28
29
30
31
32
33
34
35
36
37
38
39
40
41
42
43
44
45
46
47
48
49
50
51
52
53
54
55
56
57
58
59
60

139 *m/z* 300-1,500, 0.1 s acquisition for precursor intensities above 100,000 counts, for signals of lower
140 intensities down to 1,000 counts acquisition time increased linear to 1s, the collision energy and
141 isolation width settings were automatically calculated using the Auto MSMS fragmentation table; 5
142 precursor ions, absolute threshold 1,000 counts, preferred charge states: 2 – 4, singly charged ions
143 excluded. 1 MS/MS spectrum was acquired for each precursor and former target ions were excluded
144 for 30 s. The data output was in the MASCOT (Matrix Science Ltd, Baker Street, London, UK) .dat file
145 format. The .dat files selected used the following modification searches and parameters:
146 Fixed modification: Carbamidomethyl (C) and variable modifications: Acetyl (Protein N-term),Gln-
147 >pyro-Glu (N-term Q),Glu->pyro-Glu (N-term E),Oxidation (M).
148 Massvalues: Monoisotopic, protein Mass: Unrestricted, peptide Mass Tolerance : ± 10 ppm,
149 fragment Mass Tolerance: ± 0.1 Da and max Missed Cleavages : 1
150 The spectral data have been searched against the IPI mouse database (55272 sequences; 24903527
151 residues, all data have been filtered to show only peptide matches with an expect value of 0.05 or
152 lower.
153 These data were then processed using Scaffold 4 (version 4.0.4) proteomic software tool for
154 visualisation and analysis of the LC-ESI-MS/MS data (<http://www.proteomesoftware.com/>). The data
155 files (.dat) produced from MASCOT, which corresponded to each digested analysed, were uploaded
156 individually. Analysis with X! Tandem was selected in order to improve protein identifications with
157 searching through an additional database.
158 The following information includes the parameters and database and thresholds applied by Scaffold
159 4 version 4.0.4; database employed was the ipi.MOUSE.v3.46 database, the number of proteins was
160 55272, the search engine (as above) was MASCOT version 2.3.02. The fragment tolerance – 0.100 Da
161 (monoisotopic), parent tolerance – 10.0 ppm (monoisotopic), fixed modifications - +57 on C
162 (carbamidomethyl), variable modifications were -18 on n (pyro-glu), -17 on n (pyro-cmC), +16 on M

(oxidation) and +42 on n (acetyl). The maximum missed cleavages were 1. The peptide thresholds were 90% minimum and protein thresholds were 99% minimum, 2 peptides minimum.

Statistical analysis

Principle Component Analysis (PCA) and Partial Least Squares Discriminant Analysis (PLSDA) were performed using MATLAB® (Matrix Laboratory) (MathWorks, Inc., Natick, MA 486 USA) in conjunction with the Eigenvector PLS_Toolbox. The PCA and PLSDA statistics are representative of the fs188 data using biological replicates (in triplicate) per time point with 6 technical replicates for each biological repeat *i.e.* 414 spectra in total.

PCA and PLSDA data pre-processing using Waters MassLynx™ Software and MATLAB®

Technical spectral replicates (6 per biological replicate) were selected from the MALDI-MSI chromatogram and MS results were then imported into MATLAB® in .txt format after application of “automatic peak detection” to achieve centroidal peak information using the instrument data processing software (Waters MassLynx™ Software). Normalisation (2 - Norm) and mean centre were selected and “contiguous blocks” was used for cross validation.

Protein network analysis

Accession lists generated by results from the LC-ESI-MS/MS Mascot searches were imported into the STRING 9.0 database. Observations of the relationships were made between the proteins identified throughout a fs188 time course. The sample data was used to build predictive proteomic pathways and study the predicted functional partners of known protein-protein interactions (<http://string-db.org/>).

Immunohistochemical staining

Chemicals and Materials

Methanol, acetone, hydrogen peroxide solution 30% wt., xylene, ethanol, Gill's haematoxylin and DPX mountant were all purchased from Sigma Aldrich UK. Phosphate buffer saline tablets (Dulbecco

1
2
3
4
5
6
7
8
9
10
11
12
13
14
15
16
17
18
19
20
21
22
23
24
25
26
27
28
29
30
31
32
33
34
35
36
37
38
39
40
41
42
43
44
45
46
47
48
49
50
51
52
53
54
55
56
57
58
59
60

`A' Tablets) were from Oxoid Ltd. Normal goat serum, ImmEdge hydrophobic barrier pen, 10X casein solution, avidin/biotin horseradish peroxidase complex blocking kit, ABC solution kit, diaminobenzidine (DAB) substrate kit were from Vector Laboratories Ltd UK. Plectin antibody was from Abcam, Cambridge UK.

Immunohistochemical methods

Mounted frozen tissue sections were allowed to equilibrate to room temperature for 5 minutes. Slides were then fixed in ice-cold acetone for 20 min then rinsed in PBS. Endogenous peroxidases were blocked using 30% H₂O₂ and methanol for 20 min. After rinsing in PBS, tissues were blocked for 1hr using goat sera containing 10% casein. After PBS washes, Primary antibody (Ab) was added and left overnight at 4°C. Primary antibody concentration was optimised using a range of dilutions (1:50 - 1:1600). After overnight incubation and subsequent PBS washes, secondary Ab was added, diluted (1:200) in 2% goat sera and left for an incubation time of 1h at room temperature. After this period, ABC solution was added after rinsing in PBS and left to incubate for 45min at room temperature. After PBS washing, DAB solution was applied and left to allow development of the staining. Slides were rinsed in tap water prior to immersion in Gill's haematoxylin for 2min. After slide dehydration using 70% - 100% EtOH, tissue was immersed in 2 changes of xylene for 5 min each. Slides were mounted using DPX mountant (Sigma Aldrich, UK).

Protein precipitation and digestion

Chemicals and materials

Chloroform (CHCl₃), methanol (MeOH), acetonitrile (ACN), hydrochloric acid (HCl), tri-fluoroacetic acid (TFA), ammonium bicarbonate, DL-Dithiothreitol solution, Iodoacetamide, urea, potassium dihydrogen phosphate (KH₂PO₄), TRIzol were from Sigma-Aldrich (Dorset, UK). Modified sequence grade trypsin (20µg lyophilised) was obtained from Promega (Southampton, UK).

210 Tissue homogenisation and precipitation of protein

211 The fs188 tumour tissue was homogenised in 800µl of TRIzol solution using a micro-homogeniser
212 [10]. Homogenised solution was centrifuged (1,500 rpm) for 5 min to pellet out nuclei/ unbroken
213 cells. Post-nuclear supernatant was then centrifuged (14,000 rpm) for 30 min. Resulting supernatant
214 was discarded and cellular membrane pellet was retained for protein precipitation. 200µl of MeOH
215 and 50µl of CHCl₃ were then added to each protein pellet sample. After vortexing, 150µl HPLC H₂O
216 was added with further vortexing. After centrifugation (14,000 rpm) for 2 min, the bottom CHCl₃
217 layer was removed. A further 50µl CHCl₃ was added, removal of the bottom CHCl₃ layer was repeated
218 following centrifugation (14,000 rpm) for 2 min. Subsequent removal of the H₂O layer resulted in the
219 remaining protein precipitate layer. CHCl₃ (50µl) and MeOH (150µl) were added directly to the
220 protein precipitate, after vortexing solution was centrifuged (14,000 rpm) for 2 min. Supernatant
221 was removed and the protein pellet was then allowed to air dry for 2 min.

222 Protein Digestion

223 100µl of 0.1% RapiGest in 50mM NH₄HCO₃ buffer (pH 7.8) was added to the air-dried protein pellet.
224 Each sample pellet/ solution was consecutively vortexed, incubated at -80°C (~ 1hr) and heated to
225 70°C (1 min) until solubilised. Once fully solubilised the sample was heated to 100°C (2 min) and
226 then left to reach room temperature. Each sample was reduced with dithiothreitol (DTT) (final
227 concentration 5mM) for 30 min at 60°C the left to reach room temperature. Solutions were then
228 alkylated with iodoacetamide (final concentration 15mM) in the dark for 30 min at room
229 temperature. Sequence grade modified trypsin was added (20µg/ml) to 80µg of protein, following
230 the BCA Protein Assay (see 3.3.9) used for protein determination. In-solution digests were incubated
231 over night at 37°C with shaking.

232 Preparation of samples for column loading

233 HCl (final concentration 100mM) was added to the overnight fs188 digest. The solution was then
234 incubated for a further 45 min at 37°C. The sample was then centrifuged (14,000 rpm, 4°C) for 10

1
2
3
4
5
6
7
8
9
10
11
12
13
14
15
16
17
18
19
20
21
22
23
24
25
26
27
28
29
30
31
32
33
34
35
36
37
38
39
40
41
42
43
44
45
46
47
48
49
50
51
52
53
54
55
56
57
58
59
60

235 min and the supernatant removed for analysis. This remaining solution was lyophilised and stored at
236 -80°C until further use.

237 **Protein estimation – BCA assay**

238 **Chemicals and materials**

239 BCA protein assay reagent (bicinchoninic acid), copper (II) sulfate pentahydrate 4% solution, protein
240 standard solution, 1.0 mg/mL bovine serum albumin (BSA) were from Sigma Aldrich UK. RapiGest
241 detergent solution was purchased from Waters (UK).

242 **BCA method**

243 Solubilised protein pellets were thawed, vortexed and centrifuged ready for the BCA assay. BSA
244 standards were prepared within an analytical range of 0-4 mg/ml. BCA reagent was added to BCA
245 standards and tumour tissue solution samples and left to incubate at R/T for 30min. BCA standards
246 were measured in triplicate and samples were measured in duplicate in a 96 well plate using a
247 Wallac plate reader (spectrophotometer) at 570nm.

248 **Results and Discussion**

249 Figure 1 shows peptide mass fingerprints (as a summed spectrum from a representative tumour at
250 each time point) from *on tissue* digestion of samples throughout the fs188 post CA-4P treatment
251 time-course studied. The samples shown range from control/saline-treated to 72h post CA4P
252 administration and were acquired using MALDI-IMS-MS. From a simple visual examination of the
253 peptide mass fingerprints (Figure 1) identification of the changes occurring in the tumours following
254 treatment with CA-4P is problematic. However it would be expected that stress responses would be
255 observed and to test this supposition, ion images corresponding to peptides arising from the
256 digestion of stress response proteins were constructed. As an example of this the images in Figure 2
257 (a) – (b) display a MALDI-MSI time course for a HSP-90 peptide at m/z 1168. The images for HSP-90
258 indicate increased expression toward the 24h treatment, a response similar to the haemoglobin ion

259 at m/z 1819. These data indicate possible evidence of a 'switch back to viability' in the 72h post
260 CA4P time point.

261 In order to mine the data further Principle Component Analysis (PCA) and Partial Least Squares
262 Discriminant Analysis (PLSDA) were employed to enable classification between each time point.

263 The multivariate statistical technique of PCA was selected to provide an unbiased representation of
264 the data generated from this proteomic response study, with PLSDA providing the element of
265 discrimination allowing analysis between preselected time point results based on the PCA loadings
266 plot outcome. Principle Component Analysis was employed to help determine groupings and
267 similarities between the treatment time course data acquired via MALDI-MSI. The PCA in Figure 3(a)
268 indicated the complex inter-grouping between tumour time points and replicates. Various sample
269 groups share quadrants of the scores plot region with some groups positioned across two regions of
270 the plot causing a merger between adjacent sample replicates. The loadings plot in Figure 3(b) did
271 display separation of ions between plot regions with two ions relating to histone 2A and histone H3
272 positioned in the area relating to the later time points.

273 For PLSDA, 3 biological repeats per tumour time point were used, via MALDI-MSI acquisitions and 6
274 technical spectral repeats were taken from each biological replicate. Peak lists were exported from
275 the instrument acquisition software and imported into MATLAB using the Eigenvector PLS_Toolbox.
276 Predictive mathematical models were then built after selection of PLSDA, with the aim of observing
277 any classification between tumour time-points. Figure 4 shows the classification between Control
278 and 0.5h post-CA4P and Control and 24h post-CA4P respectively. Peaks corresponding to histone H3
279 (m/z 1032) and actin (m/z 1198) appear to be the most obvious differences between the control and
280 0.5h post CA4P PLSDA regression vector plots. Whereas in the control versus 24h post CA4P plot,
281 additional peaks assigned to histone 2A (m/z 944) and haemoglobin (m/z 1274, m/z 1416 and m/z
282 1529) are readily observable.

1
2
3
4
5
6
7
8
9
10
11
12
13
14
15
16
17
18
19
20
21
22
23
24
25
26
27
28
29
30
31
32
33
34
35
36
37
38
39
40
41
42
43
44
45
46
47
48
49
50
51
52
53
54
55
56
57
58
59
60

283 The complexity of the whole sample cohort meant that no clear groupings were observable in the

284 PCA scores plot (Figure 3a). The scores plot revealed various inter-grouping and sharing of the PCA

285 score plot quadrants by the sample replicates indicating a need for further classification between

286 sample groups.

287 PLSDA models (Figure 4a) were built to compare the treatment time points against the control

288 tumour tissue.

289 There are numerous peaks in the low mass range seen here in the regression vector plots especially

290 in the control tissue PLSDA vector plots. The peptide corresponding to actin was seen to increase in

291 the 0.5h treatment. Kanthou and Tozer [18] showed that actin stress fibres developed in human

292 umbilical vein endothelial cells at short times post CA4P administration. The results from this study

293 showed an increase of filamentous actin over time after treatment, consistent with this finding.

294 In the 24h post-treatment sample (Figure 4b), the appearance of the Hb peaks can be seen in the

295 PLSDA regression vector plot. The actin peak remains increased in relation to the control vector plot

296 with the same true for histone H3. Histone 2A is now also observed, possibly reflecting the

297 occurrence of cellular necrosis and DNA damage as a result of CA4P administration.

298 A link between increased tumour hypoxia (due to vascular shut-down) and histone H3 could be an

299 explanation for the m/z 1032 peak observed in the regression vector plots of the fs188 tumour

300 tissue [14].

301

302 Figure 5 shows display the quantitative comparison of the expression of proteins showing response

303 to treatment post-CA4P. The results shown here were selected from the many proteins identified

304 using LC-ESI-MS/MS ($n=1$), based on their relevance to the cytoskeleton, their involvement in

305 tumour stress response, or because they displayed a high percentage variability throughout the time

306 course studied. These data were generated using normalised spectrum counts from the proteomic

software tool Scaffold 4 version 4.0.4. The zoomed in region highlights the response given by the protein α -2 macroglobulin.

Table 1 details the proteins presented in Figure 5 displaying the protein accession number, number of unique peptides identified and % sequence coverage identified from MS/MS data generated.

An example MS/MS spectrum of plectin, produced using Scaffold 4 software, is shown in Figure 6 with corresponding normalised spectrum counts graph insert. A full optical scan is also featured of a 72h plectin immunohistochemical tissue section, displaying the staining of the viable tumour tissue regions. The plectin MALDI-MSI time course of a peptide ion at m/z 977 shows the marked abundance of plectin in the Control/untreated tumour compared to the later time points. Quantitative analyses of structural and stress-related proteins identified in MALDI-MSI are shown in the label free normalised spectrum graph here in Figure 6. The proteins plectin and tubulin, involved in structural integrity, are decreased over time compared to stress proteins HSP-90 and GRP-78 that increase over time.

The Scaffold 4 version 4.0.4 proteomics software tool was used for the analysis of the label free LC-ESI-MS/MS time course experimental data. Time-course protein responses were plotted using normalised spectral counting calculated and presented via Scaffold 4 version 4.0.4. The rationale for selection of the proteins included in Figure 5 was to include proteins that either had a high percentage of co-variance throughout the time course *i.e.* $\geq 100\%$, provided a known validating response or were of relevance to the stress response in tumours.

The increased abundance observed in Figure 5 for both haemoglobin subunit alpha and haemoglobin subunit beta-2 is indicative of the distinctive gross pharmacological response arising from the administration of a vascular disrupting agent *i.e.* haemorrhagic necrosis.

Heat shock protein 90 (HSP-90) is ubiquitous in all normally functioning cells and serves to prevent the misfolding of proteins by helping to retain the correct structural format of the protein [15]. HSP-

1
2
3
4
5
6
7
8
9
10
11
12
13
14
15
16
17
18
19
20
21
22
23
24
25
26
27
28
29
30
31
32
33
34
35
36
37
38
39
40
41
42
43
44
45
46
47
48
49
50
51
52
53
54
55
56
57
58
59
60

331 90 has been suggested as a potential target protein for anticancer therapy due to the cancer cell's
332 dependence on this protein for structural conformity [16]. It is known that inhibition of HSP-90
333 results in the degradation of the HSP-90 stabilised protein (client protein) via the proteasome.

334 Elevated levels of HSP-90 in breast cancer patients have been found to correlate with poor patient
335 survival due to the conserving effect of HSP-90 on human epidermal growth factor receptor 2 [17].
336 HSP-90 is commonly highly expressed in solid tumours and plays a key role in the evasion of
337 apoptosis thus promoting tumour cell survival [16]. The presence of HSP-90 is shown throughout the
338 MALDI-MSI fs188 time course in Figure 2 and label free normalised spectrum counts graph in Figure
339 5. The MALDI image corresponding to 24hr post-CA4P (Figure 2) indicates very high levels of HSP-90
340 at this time, suggesting a protective role against protein misfolding during recovery. The possible
341 '*switch back to viable tissue*' appears to be exhibited by the MALDI-MSI 72h time point in Figure 2a
342 and b as a reduction in HSP90 and Hb expression.

343 The data shown in Figure 5 also demonstrates the disruption in the architectural integrity of the
344 vasculature as indicated by decreases in structural tubulin beta-5 chain and tubulin alpha-1B chain
345 compared to the control tumour tissue.

346 Actin, cytoplasmic 1(Beta-actin) and actin, alpha skeletal muscle precursor (Alpha-actin-1) appear to
347 show different trends throughout the LC-ESI-MS/MS data (Figure 5). It is known that the
348 reorganisation and/or disruption of the cytoskeleton results in stress fibre formation [18] that could
349 explain an increase in beta-actin in the 0.5h time point (Figure 5) in response to the drug. Over time,
350 the tumour appears to recover, favouring actin polymerisation after a brief decrease of beta-actin in
351 the 6h time point, with increased levels evident at 24h and 72h post CA4P administration.

352 The role of progenitor cells and/or infiltrating immune cells in tumour response to treatment is
353 receiving a great deal of attention. Recently, it was shown that a Tie-2 expressing sub-population of
354 macrophages was increased after CA4P treatment, in two mouse models of breast cancer [19] and

that these contributed to resistance to CA4P treatment. Alpha-2-macroglobulin is known to be synthesised locally in tissues by infiltrating macrophages. It is a carrier protein and is also known to be linked to growth factors and cytokines i.e. basic fibroblast growth factor, Interleukin 1- β (IL-1 β) and transforming growth factor beta [20, 21].

The dose response relationship of alpha-2-macroglobulin from the LC-ESI-MS/MS results can be observed in the Figure 5 insert. Alpha-2-macroglobulin was not detected in the early fs188 treated time points but a sudden increase is evident from 6 hours, with a surge at the 24h time point and then a drop in expression at 72 hours (Figure 5). Alpha-2-macroglobulin levels may reflect numbers of infiltrating immune cells. However, attempts to validate this possibility by immunohistochemical staining for the macrophage cell surface marker, F4/80, were inconclusive due to inter-tumour variability in staining levels (results not shown). The steep increase of alpha-2-macroglobulin at 24h, followed by a decrease at 72 h, follows the pattern of increased and resolving tumour necrosis, found at these time-points, and may relate to phagocytic activity of the macrophage tumour population.

Plectin (Figure 5 and 6) was found to have a high value of percentage co-variance (170%) of response throughout the sample time-course. LC-ESI-MS/MS data (Figure 5) indicated a marked abundance of plectin in the untreated tumours and decreased levels by 0.5 h after CA4P treatment, with very low levels thereafter. The MALDI-MSI data for plectin showed a very similar pattern (Figure 6). As further confirmation of this response, immunohistochemical studies using a plectin antibody were performed to determine the expression in histological tumour sections. The plectin staining suggested that this protein is highly expressed in untreated fs 188 tumours. This agreed with both the MALDI-MSI and LC-ESI-MS/MS data. From the plectin immunohistochemistry performed it is also apparent that plectin is distributed only in viable tumour regions.

Plectin has been proposed as a novel prognostic marker for head and neck squamous cell carcinoma, linked to roles in cancer cell migration and invasion (Katada *et al* (2012). Elevated levels of plectin

1
2
3
4
5
6
7
8
9
10
11
12
13
14
15
16
17
18
19
20
21
22
23
24
25
26
27
28
29
30
31
32
33
34
35
36
37
38
39
40
41
42
43
44
45
46
47
48
49
50
51
52
53
54
55
56
57
58
59
60

380 have also been found in colorectal cancer, prostate cancer and pancreatic ductal adenocarcinoma
381 [24-27]. Results reported here suggest that CA4P greatly interferes with plectin expression. However,
382 further investigations are warranted to determine whether changes in plectin levels are simply
383 reflecting changes in necrosis following treatment or whether there are significantly different levels
384 in surviving viable tumour regions.

385 IQGAP1 is a multimodal scaffolding protein that is implemented in actin dynamics, tubulin
386 multimerisation, cell motility and migration, via numerous signalling pathways [28]. Some studies
387 reported that increased expression of IQGAP1 resulted in disruption of cell-cell junctions thus
388 promoting a migratory, invasive phenotype [29]. We have demonstrated that IQGAP1 is undetected
389 in untreated fs188 fibrosarcomas (Figure 3) but is visible from 0.5h post CA-4-P treatment, at which
390 point levels decrease through to the 72h treatment group, suggesting possible CA4P
391 pharmacological action.

392 The glycoprotein Tenascin (C), has similar functions to those of IQGAP1 having involvement in
393 tumour survival and the outgrowth of circulating cancer cells [30]. The levels of tenascin C we
394 observed (Figure 5) show an increase in the 0.5h treatment group compared to untreated controls
395 with decreases evident in the later time points post CA-4-P administration, a similar response to that
396 observed for IQGAP1. The action of CA4P does appear to have an inhibitory effect on Tenascin C.
397 However, it has been suggested that its fellow glycoprotein, Tenascin W, is more specific for
398 tumours [31]. Mass spectrometric techniques could help to ascertain the relative abundance of
399 these two proteins in tumour tissue and their response to treatment.

400 Alpha-enolase is thought to be implemented in many processes. In addition to its role as a glycolytic
401 enzyme it is known to have transcriptional capacity and molecular chaperone capabilities with
402 hypoxia being a known modulator of its expression [32-34]. CA4P treatment caused a steady
403 increase in alpha-enolase with time. Alpha-enolase is regarded as a tumour-associated antigen (TAA)
404 and when elevated levels are present in tumour tissue, activation of immune responses occurs in

patients with cancer [35]. Increased expression of Alpha-enolase is also indicative of aggressive tumour progression. Therefore, an increase in alpha-enolase after CA4P (Figure 5) could be a marker for the resistant phenotype of the fs188 tumour type, reflecting its regenerative capability.

From the LC-ESI-MS/MS time-course results in Figure 5, *Tgfb1* is shown to demonstrate a 'L' shape trend line similar to that seen for plectin (Figure 5 and 6), with high levels in untreated compared to treated tumours. The latter response is a trend similar to the results documented in an article by Li *et al* (2012) [36]. *Tgfb1* may have a dual role; an anti-tumourigenic function in early tumour growth and as a pro-oncogenic supporter in late stage tumours. Therefore the significance of the CA4P-induced changes shown in our study remains to be determined.

Figure 7 shows the immunohistochemical staining of plectin in the fibrosarcoma tissue in Control/untreated (Figure 7a), 6h (Figure 7b) and 24h (Figure 7c) post CA4P. The staining for plectin in the untreated tissue is widely spread and intense throughout the tissue. The emergence of necrotic tissue is observable in the 6h anti-plectin (and insert) image with increased necrosis visible in the 24h post CA4P section. Plectin however, appears in the viable tissue region located in the tumour periphery of the fibrosarcoma tissue. Plectin is described as a 'cytolinker' and has a key role in the stabilisation of the cytoskeleton via the formation of a mesh-like scaffold [12,. 13].

The proteomic pathway tool String 9.0 was used to depict the relationships between proteins featured earlier. Figure 8 shows direct links between proteomic 'bubbles' and spatial associations, propose an understanding of functionality between the proteins within the network.

The MALDI peptide mass fingerprints (Figure 1) from the fs188 *on tissue* digests contain numerous peaks. The challenge here was the exploration and identification of the low abundant species present. The MALDI images in Figure 2 are examples of how the spatial distribution and ion intensities can differ greatly across the treatment time course.

428

1
2
3
4
5
6
7
8
9
10
11
12
13
14
15
16
17
18
19
20
21
22
23
24
25
26
27
28
29
30
31
32
33
34
35
36
37
38
39
40
41
42
43
44
45
46
47
48
49
50
51
52
53
54
55
56
57
58
59
60

Visualisation of the complex protein pathways and networks that govern tumour biological function helps the understanding of protein dose response relationships. String 9.0 (<http://string-db.org/>) was used to visualise protein-protein interactions in the data reported here. Protein-protein interactions visualised by String 9.0, are depicted by spatial positioning and linear connections with thicker lines representing stronger associations between proteins. The focal pathway association seen here (Figure 8) within this group of proteins is the linkage between the heat shock proteins; HSP-90 α , HSP-90 β , GRP-78 (Hspa5) and Actin, cytoplasmic 1 and Ras GTPase-activating-like protein (IQGAP1). The stronger association within this pathway runs directly from HSP-90 α through to IQGAP1 encompassing Actin, cytoplasmic 1. The latter is characteristic of an active tumour micro-environment incorporating the morphological changes exhibited by architectural remodelling of actin due to CA4P administration. Although not directly linked, plectin and tenascin display close positioning to IQGAP1, all of which as previously mentioned, are known to be involved with promoting tumour survival, cellular migration and metastatic invasion. A strong link is visible between fellow tubulin proteins. Interestingly, alpha-enolase (ALO22784) is in close proximity to carrier protein alpha-2-macroglobulin (A2m). Close positioning of ALO22784 to macrophage related protein A2m is indicative of allergic stress response, which remains true to the pharmacological intervention here post CA4P administration [40]. Haemoglobin subunit beta positioned above (A2m and ALO22784) supports the haemorrhagic action of CA-4-P. Tumour suppressing adhesion protein transforming growth factor-beta-induced protein ig-h3 (Tgfb β), is joined in this structural reorganisational milieu. As mentioned above, this protein is involved in cell-collagen interactions.

The data reported here shows an active tumour response to CA4P. Collectively, the results from the LC-ESI-MS/MS comprise of proteins connected with necrosis, cell structural reorganisation and actin polymerisation but also tumour survival and stress-induced molecular chaperones. The inverse correlation of molecular chaperone HSP-90 and survival-promoting plectin is evidence of this. The gross changes in expression were detectable by LC-ESI-MS/MS, with the distinct regional differences in the tissue being observable in the MALDI-MSI and immunohistochemistry data.

Overall the levels of the proteins involved in stress responses i.e. GRP-78, HSP-90 β , HSP-70 are increased over time, but interestingly expression of HSP-90 α was reduced in the 72h treatment sample, possibly highlighting the switch back to tumour viability in this stage post-CA4P administration, as can be seen from viable tissue regeneration in histological sections. The latter may be a reflection of another tumour cell population surpassing the protective role of HSP-90 resulting in tumour rejuvenation. For the future, it will be important to examine potentially subtle proteomic differences between untreated viable and regenerating viable tumour regions.

Concluding Remarks

A combination of MALDI-MSI, LC/MS/MS and IHC has been used to study protein induction in a mouse fibrosarcoma model following treatment with CA4P, a vascular disrupting agent. Analysis of the MALDI-MSI data by multivariate statistics revealed gross changes in protein response indicative of stress and necrotic haemorrhaging. These findings were validated by the LC/MS/MS and IHC data. Analysis of the LC/MS/MS data also revealed changes in expression of other cancer significant proteins e.g. plectin and HSP90. It was possible to then plot images of peptides of these proteins within the original MALDI-MSI data set to demonstrate their regional distribution. An inverse correlation between the expression of structural and stress response proteins over the time-course experiment was observed and proteins that distinguished the viable tumour region were identified. The use of multiple technologies to validate the findings was found to be essential for confidence in MALDI-MSI data.

Acknowledgements

Adam Dowle is gratefully acknowledged for carrying out the LC/MS/MS experiments at the Proteomics Technology Facility, Department of Biology (Area 15), University of York. This work was funded by Programme Grant C1276/A10345 from Cancer Research UK and EPSRC with additional

1
2
3
4
5
6
7
8
9
10
11
12
13
14
15
16
17
18
19
20
21
22
23
24
25
26
27
28
29
30
31
32
33
34
35
36
37
38
39
40
41
42
43
44
45
46
47
48
49
50
51
52
53
54
55
56
57
58
59
60

478 funding from MRC and Department of Health England. We thank Professor Bob Pettit, Arizona State
479 University for the supply of CA4P.
480

For Peer Review

481 **References**

482 [1]Tozer, G. M., Akerman, S., Cross, N. A., Barber, P. R., Björndahl, M. A., Greco, O., Harris, S., Hill,
483 S. A., Honess, D. J., Ireson, C. R., Pettyjohn, K. L., Prise, V. E., Reyes-Aldasoro, C. C., Ruhrberg, C.,
484 Shima, D. T., Kanthou, C. (2008) Blood Vessel Maturation and Response to Vascular-Disrupting
485 Therapy in Single Vascular Endothelial Growth Factor-A Isoform-Producing Tumours. *Cancer*
486 *Research*. 68, 2301–11

487

488 [2] Cole, L. M., Djidja, M-C., Bluff, J. E., Claude, E., Carolan, V. A., Paley, M., Tozer, G. M., Clench, M.
489 R (2011) Investigation of protein induction in tumour vascular targeted strategies by MALDI MSI.
490 *Methods*. 54, 442–453

491

492 [3] Schwartz, S. A., Wei, I. R. J., Johnson, M. D., Toms, S. A., Caprioli, R. M. (2004) Protein profiling
493 in brain tumors using mass spectrometry: feasibility of a new technique for the analysis of protein
494 expression. *Clinical Cancer Research: an official journal of the American Association for Cancer*
495 *Research*. 10, 981–987

496

497 [4] Chaurand, P., DaGue, B. B., Pearsall, R. S., Threadgill, D. W., Caprioli, R. M. (2001) Profiling
498 proteins from azoxymethane-induced colon tumors at the molecular level by matrix-assisted laser
499 desorption/ionization mass spectrometry. *Proteomics*. 1, 1320–1326

500

501 [5] Lemaire, R., Desmons, A., Tabet, J. C., Day, R., Salzet, M., Fournier, I. (2007) Direct analysis
502 and MALDI imaging of formalin-fixed, paraffin-embedded tissue sections. *Journal of Proteome*
503 *Research*. 6, 1295–1305

1
2
3
4
5
6
7
8
9
10
11
12
13
14
15
16
17
18
19
20
21
22
23
24
25
26
27
28
29
30
31
32
33
34
35
36
37
38
39
40
41
42
43
44
45
46
47
48
49
50
51
52
53
54
55
56
57
58
59
60

504 [6] Schwamborn, K., Krieg, R. C., Reska, M., Jakse, G., Knuechel, R., Wellmann, A. (2007)
505 Identifying prostate carcinoma by MALDI-Imaging. *International Journal of Molecular Medicine*. 20,
506 155–159
507
508 [7] Lemaire, R., Menguellet, S. A., Stauber, J., Marchaudon, V., Lucot, J., Collinet, P., Farine, M.,
509 Vinatier, D., Day, R., Ducoroy, P., Salzet, M., Fournier, I. (2007) Specific MALDI Imaging and
510 Profiling for Biomarker Hunting and Validation: Fragment of the 11S Proteasome Activator Complex,
511 Reg Alpha Fragment, Is a New Potential Ovary Cancer Biomarker. *Journal of Proteome Research*. 6,
512 4127–4134
513
514 [8] Shimma, S., Furuta, M., Ichimura, K., Yoshida, Y., Setou, M., (2006) A Novel Approach to in situ
515 Proteome Analysis Using Chemical Inkjet Printing Technology and MALDI-QIT-TOF Tandem Mass
516 Spectrometer. *Journal of Mass Spectrometry Society Japan*. 54, 133–140
517
518 [9] Groseclose, M. R., Andersson, M., Hardesty, W. M., Caprioli, R. M. (2007) Identification of
519 proteins directly from tissue: in situ tryptic digestions coupled with imaging mass spectrometry.
520 *Journal of Mass Spectrometry*. 42, 254–262
521
522 [10] Workman P., Aboagye E. O., Balkwill F., Balmain A., Bruder G., Chaplin D. J., Double J. A.,
523 Everitt J., Farningham D. A. H., Glennie M. J., Kelland L. R., Robinson V., Stratford I. J., Tozer G. M.,
524 Watson S., Wedge S. R., Eccles S. A., and An ad hoc committee of the National Cancer Research
525 Institute (2010) *British Journal of Cancer*. 102, 1555–1577

- [10] Kline KG and Wu CC (2009) MudPIT analysis: application to human heart tissue. *Methods in Molecular Biology*. 528, 281-93
- [11] Ossege, L.M., Voss, B., Müller, K. M. (1994) Expression and secretion of alpha-2-macroglobulin by dust-stimulated alveolar macrophages. *Pneumologie*. 48, 236-9
- [12] Liu, Y-H., Ho, C-C., Cheng, C-C., Chao, W-T., Pei, R. J., Hsu, Y-H., Lai, Y-S. (2011) Cytokeratin 18-mediated disorganization of intermediate filaments is induced by degradation of plectin in human liver cells. *Biochemical and Biophysical Research Communications*. 407, 575–580
- [13] Wiche, G. (1998) Role of plectin in cytoskeleton organization and dynamics. *Journal of Cell Science*. 111, 2477–2486.
- [14] Wang Z, Yang D, Zhang X, Li T, Li J, Tang Y, Le W (2011) Hypoxia-Induced Down-Regulation of Nepilysin by Histone Modification in Mouse Primary Cortical and Hippocampal Neurons. *PLoS ONE*. 6., e19229
- [15] Neckers, L (2007) Heat shock protein 90: The cancer chaperone. *Journal of Biosciences*. 32, 517–530
- [16] Den, R. B. and Lu, B. (2012) Heat shock protein 90 inhibition: rationale and clinical potential. *Therapeutic Advances in Medical Oncology*. 4, 211–218

1
2
3 548
4
5
6 549 [17] Jameel, A., Skilton, R. A., Campbell, T. A., Chander, S. K., Coombes, R. C., Luqmani, Y. A.
7
8 550 (1992) Clinical and biological significance of HSP89 alpha in human breast cancer. International
9
10 551 *Journal of Cancer*. 50, 409–415
11
12
13 552
14
15
16 553 [18] Kanthou, C., Tozer, G. M. (2002) The tumour vascular targeting agent combretastatin A-4-
17
18 554 phosphate induces reorganization of the actin cytoskeleton and early membrane blebbing in human
19
20 555 endothelial cells. *BLOOD*. 99, 2060-2069
21
22
23 556
24
25
26 557 [19] Welford, A. F., Biziato, D., Coffelt, S. B., Nucera, S., Fisher, M., Pucci, F., Di Serio, C., Naldini,
27
28 558 L., De Palma, M., Tozer, G. M , Lewis, C. E . (2011) TIE2-expressing macrophages limit the
29
30 559 therapeutic efficacy of the vascular-disrupting agent combretastatin a4 phosphate in mice. *The*
31
32 560 *Journal of Clinical Investigation*. 121, 1-5
33
34
35
36 561
37
38
39 562 [20] Feige, J. J., Negoescu, A., Keramidas, M., Souchelnskiy, S., Chambaz, E. M. (1996) Alpha 2-
40
41 563 macroglobulin: a binding protein for transforming growth factor-beta and various cytokines.
42
43 564 *Hormone research*. 45, 227-32
44
45
46 565
47
48
49 566 [21] Wellcome trust Sanger Institute (2012) Available at URL:
50
51 567 <http://pfam.sanger.ac.uk/family/PF01835>). Last accessed 22/01/13.
52
53
54 568
55
56
57
58
59
60

- 569 [22] Ey, L., Li, J. F., Gnatovskiy, L., Deng, Y., Zhu, L., Grzesik, D. A., Qian, H., Xue, X. N., Pollard, J.
570 W. (2006) Macrophages regulate the angiogenic switch in a mouse model of breast cancer. *Cancer*
571 *Research*. 66, 11238–11246
572
- 573 [23] Bingle, L., Brown, N. J., Lewis, C. E. (2002) The role of tumour associated macrophages in tumour
574 progression: implications for new anticancer therapies. *The Journal of Pathology*. 196 254–265
575
- 576 [24] Winter, L. and Wiche, G. (2013) The many faces of plectin and plectinopathies: pathology and
577 mechanisms. *Acta Neuropathologica*. 125, 77–93
578
- 579 [25] Nagle, R. B., Hao, J., Knox, J. D., Dalkin, B. L., Clark, V., Cress, A. E. (1995) Expression of
580 hemidesmosomal and extracellular matrix proteins by normal and malignant human prostate tissue.
581 *American Journal of Pathology*. 146, 1498–507
582
- 583 [26] Lee, K. Y., Liu, Y. H., Ho, C. C., Pei, R. J., Yeh, K. T., Cheng, C. C., Lai, Y. S. (2004) An early
584 evaluation of malignant tendency with plectin expression in human colorectal adenoma and
585 adenocarcinoma. *Journal of Medicine*. 35, 141–149
586
- 587 [27] Katada, K., Tomonagab, T., Satoh, M., Matsushita, K., Tonoikea, Y., Koderad, Y., Hanazawa ,
588 T., Nomura, F., Okamotoa, Y. (2012) Plectin promotes migration and invasion of cancer cells and is
589 a novel prognostic marker for head and neck squamous cell carcinoma. *Journal of Proteomics*. 1803-
590 1815

1
2
3 591
4
5
6 592 [28] Malarkannan, S., Awasth, A., Rajasekaran, K., Kumar, P., Schuldt, K. M., Bartoszek, A.,
7
8 593 Manoharan, N., Goldner, N. K., Umhoefer, C. M., Thaka, M. S. (2012) IQGAP1: A Regulator of
9
10 594 Intracellular Spacetime Relativity. *The Journal of Immunology*. 188, 2057-2063
11
12
13 595
14
15
16 596 [29] Mataraza, J. M., Briggs, M. W., Zhigang, L., Entwistle, A., Ridley, A. J., Sacks, D. B. (2003)
17
18 597 IQGAP1 Promotes Cell Motility and Invasion. *The Journal of Biological Chemistry*. 278, 41237–41245
19
20
21 598
22
23
24 599 [30] Oskarsson, T., Acharyya, S., Zhang, X. H-F., Vanharanta, S., Tavazoie, S., Morris, P. G., Downey,
25
26 600 R. J., Manova-Todorova, K., Brogi, E., Massague, J. (2011) Breast cancer cells produce Tenascin C as
27
28 601 a metastatic niche component to colonize lungs. *Nature Medicine*. 17, 867-874
29
30
31 602
32
33
34 603 [31] Brellier, F., Martina, E., Degen, M., Heuzé-Vourc'h, N., Petit, A., Kryza, T., Courty, Y.,
35
36 604 Terracciano, L., Ruiz, C., Chiquet-Ehrismann, C. (2012) Tenascin-W is a better cancer biomarker
37
38 605 than tenascin-C for most human solid tumours. *BMC Clinical Pathology*. 12, 1-10
39
40
41 606
42
43
44 607 [32] Pancholi, V. (2001) Multifunctional α -enolase: its role in diseases. *CMLS Cellular and Molecular*
45
46 608 *Life Sciences*. 58, 902–920
47
48
49 609
50
51
52 610 [33] Kang, H. J., Jung, S-K., Kim, S. J., Chung, S. J. (2008) Structure of human α -enolase (hENO1), a
53
54 611 multifunctional glycolytic enzyme. *Acta Crystallographica Section D*. D64, 651–657
55
56
57
58 612
59
60

- 613 [34] Sedoris, K. C., Thomas, S. D., Miller, D. M. (2010) Hypoxia induces differential translation of
614 enolase/MBP-1. *BMC Cancer*. 10, 1-14
615
- 616 [35] Capello, M., Ferri-Borgogno, S., Cappello, P., Novellia, F. (2011) α -enolase: a promising
617 therapeutic and diagnostic tumor target. *FEBS Journal*, 1064–1074
618
- 619 [36] Li, B., Wen, G., Zhao, Y., Tong, J., Hei, T. K. (2012) The role of TGFBI in mesothelioma and
620 breast cancer: association with tumor suppression. *BMC Cancer*. 12, 1-12
621
- 622 [37] Kim, J. E., Kim, E. H., Han, E. H., Park, R. W., Park, I. H., Jun, S. H., Kim, J. C., Young, M. F.,
623 Kim, I. S. (2000) A TGF-beta-inducible cell adhesion molecule, betaig-h3 is downregulated in
624 melorheostosis and involved in osteogenesis. *Journal of Cellular Biochemistry*. 77, 169–178
625
- 626 [38] Zhao, Y., Shao, G., Piao, C. Q., Berenguer, J., Hei, T. K. (2004) Down-regulation of Betaig-h3
627 gene is involved in the tumorigenesis in human bronchial epithelial cells induced by heavy-ion
628 radiation. *Radiation Research*. 162, 655–659
629
- 630 [39] Shao, G., Berenguer, J., Borczuk, A. C., Powell, C. A., Hei, T. K., Zhao, Y. (2006) Epigenetic
631 inactivation of Betaig-h3 gene in human cancer cells. *Cancer Research*. 66, 4566–4573
632
- 633 [40] Gilbertson, R. J. and Graham, T. A. (2012) Cancer: Resolving the stem-cell debate. *Nature*.
634 488, 462–463

1
2
3
4
5
6
7
8
9
10
11
12
13
14
15
16
17
18
19
20
21
22
23
24
25
26
27
28
29
30
31
32
33
34
35
36
37
38
39
40
41
42
43
44
45
46
47
48
49
50
51
52
53
54
55
56
57
58
59
60

635 **Table and Figure Legends**

636 **Figure 1:** Examples of MALDI Peptide Mass Fingerprints (PMFs) from a time course study. Spectra
637 shown are Saline (Control), 0.5h, 6h, 24h and 72h post CA4P treatment of fs188 mouse
638 fibrosarcomas.

639 **Figure 2:** MALDI-MSI time course images and zoomed in mass spectra of peptides corresponding to
640 (a) HSP-90 at m/z 1168 and (b) haemoglobin at m/z 1819. The tumour tissue images here show the
641 spatial distribution of the selected ions in Control, 0.5h, 6h, 24h and 72h post CA4P treatment
642 samples. The possible switch back to viable tissue is indicated by the red arrow in the 72h sample
643 and asterisks mark the ions of interest in each zoomed spectrum

644 **Figure 3:** Principle Component Analysis (a) scores plot displaying the complex groupings and inter-
645 grouping between the full sample time course replicates, colour coded icons are as follows: 6 -
646 Control groups, 7 – 0.5h, 8 – 6h, 9 – 24h and 10 – 72h post CA4P. (b) corresponding loadings plot
647 displaying the spatial relation of each ion to the position of groupings in the scores plot (a). The two
648 arrows indicate histones 2A and H3, commonly observed in the PCA scores region relating to the
649 later time points possibly reflecting necrosis/apoptosis in the tumour tissue.

650 **Figure 4:** Partial least squares discriminant analysis (PLSDA) regression vector plot comparing MALDI
651 “on-tissue” digest data from samples of fs188 Control and 0.5h post combretastatin-4-phosphate
652 (CA4P), and Control and 24h post CA4P fs188 on-tissue digests. The blue arrows are indicative of
653 Histone 2A (m/z 944), Histone H3 (m/z 1032), Actin (m/z 1198) and the red arrows correspond to Hb
654 peaks; m/z 1274, m/z 1416 and m/z 1529.

655 **Figure 5:** A selection of fs188 time course results post CA4P treatment using LC-ESI-MS/MS. The
656 rationale for protein selection here were targets that were either relevant to the tumour stress
657 response or displayed a high percentage of normalised spectrum count variability throughout the

1
2
3 658 treatment time course after importing into proteomic software tool Scaffold. The zoomed in insert is
4
5 659 to show the response by α -2 macroglobulin. The result shown are $n = 1$.
6
7

8 660 **Figure 6:** Example MS/MS spectrum and insert showing a normalised intensity graph of plectin in
9
10 661 f188 LC-ESI-MS/MS results. A full optical scan showing the staining of Plectin in the viable tumour
11
12 662 tissue region. MALDI-MSI time course displays the intensity of plectin at m/z 977 throughout the
13
14 663 treatment points; control, 0.5h post CA4P, 6h post CA4P, 24h post CA4P and 72h post CA4P. Label
15
16 664 free graph of normalised spectrum counts to show an inverse relationship between structural
17
18 665 proteins and those thought to be involved in tumour survival and the stress response.
19
20

21
22 666 **Figure 7:** Immunohistochemical staining of Plectin in Fs188 tissue post CA4P treatment. The
23
24 667 following examples shown are part of a CA4P time course studied. (a) plectin staining of Control
25
26 668 untreated fs188 tissue, the staining is diffuse throughout the tissue here, (b) plectin staining of fs188
27
28 669 tissue 6h post CA4P treatment; at higher magnification the staining of viable tissue is clearly defined
29
30 670 in comparison to the unstained necrotic tissue, (c) plectin staining is shown to be localised in a viable
31
32 671 tissue region near the tumour edge of 188 fibrosarcoma after 24 hours CA4P treatment.
33
34
35

36 672 **Figure 8:** LC-ESI-MS/MS selected proteins of interest from fs188 tumours shown in Figure 5,
37
38 673 visualised through proteomic pathway software STRING 9.0. The interactions shown here depict
39
40 674 direct (physical) and indirect (functional) links between the proteins that were identified from
41
42 675 tryptically digested tissue homogenate.
43
44
45

46 676

47
48 677 **Table 1:** Table of protein identifications detailing protein accession number, number of unique (in
49
50 678 terms of amino acid sequence) peptides identified and % sequence coverage identified from MS/MS
51
52 679 data generated.
53
54

55
56 680
57
58
59
60

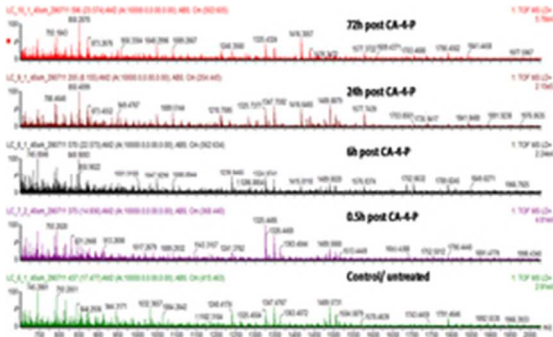
1
2
3
4
5
6
7
8
9
10
11
12
13
14
15
16
17
18
19
20
21
22
23
24
25
26
27
28
29
30
31
32
33
34
35
36
37
38
39
40
41
42
43
44
45
46
47
48
49
50
51
52
53
54
55
56
57
58
59
60

681

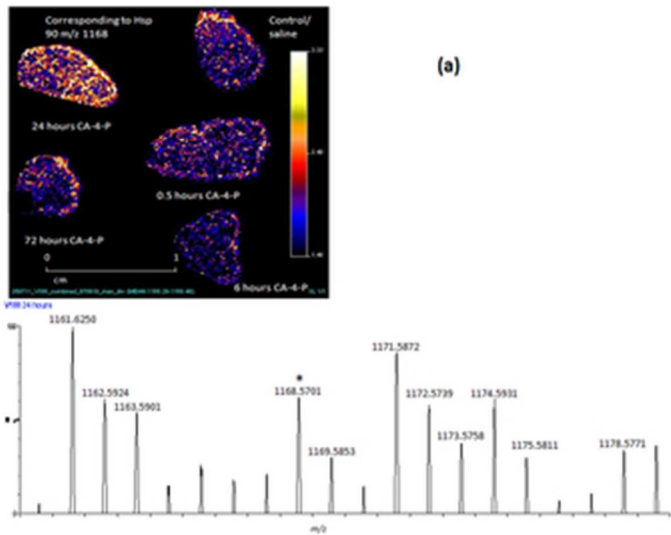
For Peer Review

protein	accession number	number of unique peptides identified	% sequence coverage identified from MS/MS
78 kDa glucose-regulated protein	IP100319992	2	5%
Actin alpha skeletal muscle	IP100110827	1	30%
Actin cytoplasmic 1	IP100110850	18	63%
Alpha-2-macroglobulin	IP100624663	1	2%
Alpha-enolase	IP100462072	6	22%
Beta-ig-h3	IP100122528	12	23%
Haemoglobin subunit alpha	IP100469114	4	42%
Haemoglobin subunit beta-2	IP100316491	3	29%
Heat shock 70 kDa protein	IP100331556	1	2%
Hsp-90 alpha	IP100330804	2	11%
Hsp-90 beta	IP100229080	7	12%
Plectin	IP100229509	73	19%
Ras GTPase-activating-like protein	IP100467447	6	6%
Tenascin	IP100420656	4	2%
Tubulin alpha-1B chain	IP100117348	11	36%
Tubulin beta-5-chain	IP100117352	15	45%

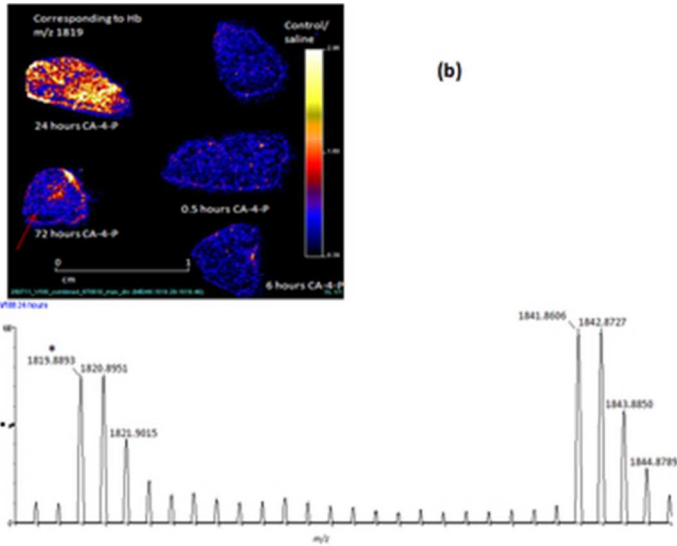
25x26mm (300 x 300 DPI)



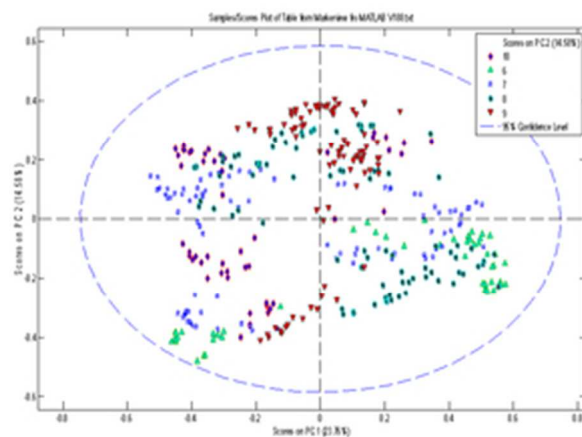
23x14mm (300 x 300 DPI)



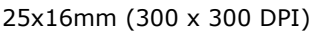
28x22mm (300 x 300 DPI)

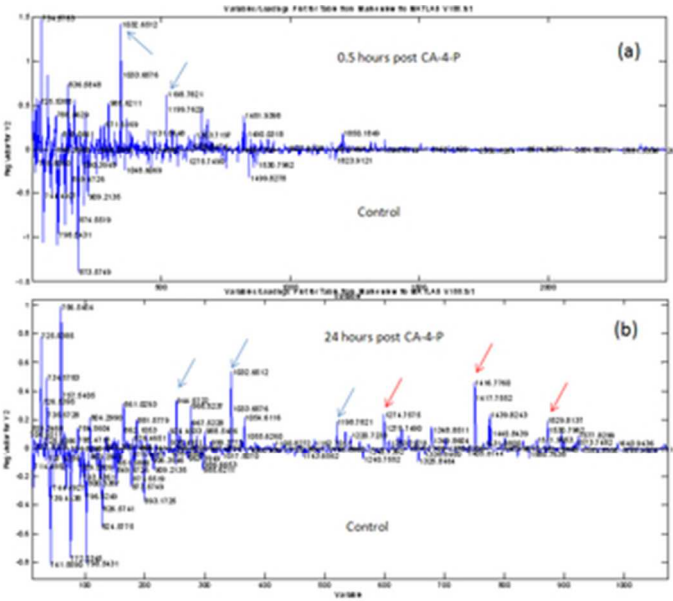


29x23mm (300 x 300 DPI)

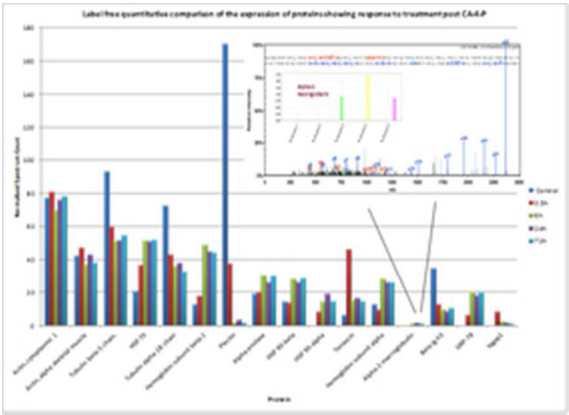


25x18mm (300 x 300 DPI)

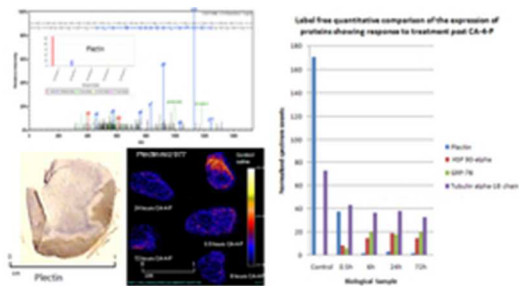




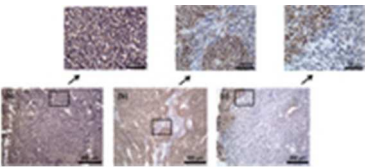
28x25mm (300 x 300 DPI)



23x17mm (300 x 300 DPI)

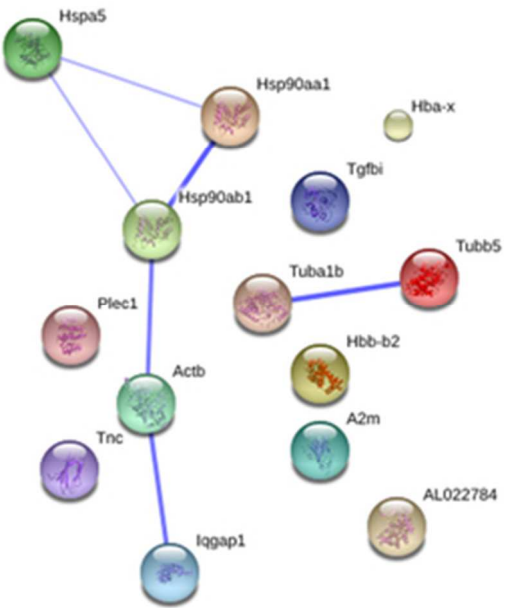


22x12mm (300 x 300 DPI)



15x6mm (300 x 300 DPI)

For Peer Review



22x26mm (300 x 300 DPI)

Review